This article has been accepted for publication in a future issue of this journal, but has not been fully edited. Content may change prior to final publication. Citation information: DOI 10.1109/TIA.2015.2477798, IEEE Transactions on Industry Applications

# Analysis of a PM Vernier Motor with Spoke Structure

Byungtaek Kim
Dept. of Electrical Engineering
Kunsan National University
Kunsan, Korea
btkim@kunsan.ac.kr

Thomas A. Lipo
Electrical and Computer Engineering
University of Wisconsin
Madison, WI, USA
lipo@engr.wisc.edu

***Abstract*— In this paper a vernier motor with a spoke PM structure instead of a surface PM is proposed in order to obtain higher power factor and flux density. However, upon investigating this structure with a single gap, unique effects which virtually eliminate the vernier effect are analytically identified. To avoid these effects and improve the power factor the spoke PM vernier motor with a double gap is then proposed. Analytic equations for back EMF and power factor are then derived for this motor in terms of various geometric factors such as the numbers of magnet and winding pole, and magnet thickness etc. For a case study, the practical achievable maximum power and power factor are calculated and verified with accurate simulations.**

## I. INTRODUCTION

A vernier machine has been recognized as being very suitable for the systems requiring low speed and high torque such as wind power generators [1] and electric vehicle motors [2]. Thus, interest in this motor has been increasing and several research results concerning this motor topology have been reported recently [3-7], in which a number of structures were proposed such as split-fractional slots, surface-interior PM and single-dual air gaps etc. In those studies, however, characteristic equations of vernier machine in analytical form with practical geometries have never suggested, which is mainly due to ambiguous permeance distribution of air gap. Consequently, this type of machine has still a variety of unexplored characteristics in spite of its somewhat lengthy history. In particular, recent work has successfully revealed previously unknown operation and design principles for the surface PM vernier motor by introducing permeance distribution in terms of practical machine's geometry [8]. According to these results, a surface PM vernier motor is shown to be able to produce more than twice the back EMF of a conventional PM motor. However, the reactance of the motor increases more than does the back EMF, causing surface magnet designs to have a poorer power factor. To overcome this problem it was stated that a new structure having a higher back EMF or lower reactance is necessary [8].

This research begins with the hypothesis established through the investigation of the previously derived back EMF [8]. It is that the back EMF will be much higher when the PM vernier motor has a spoke structure. Based on this observation, a single gap spoke type PM vernier motor is first studied in this paper. Using an equivalent magnetic circuit, the flux density distribution is analyzed and a potential oscillation phenomena in associated with such a motor is found, which is a critical problem removing the advantages of vernier effects. Next, a double gap spoke PM vernier motor is proposed as being a structure free from the critical problem found in single gap structures. In support of this assertion, a very recent research dealing with a double gap spoke PM vernier motor has been reported, which shows the improvement of power factor and density with variety of additional characteristics [9]. However this work fails to show the characteristic relationships between back EMF, power factor, and additional factors such as the number of magnets, winding pole pairs, stator slots and geometries of the machine. Hence, it is difficult to use the results of this paper for practical design. This study derive, therefore, the key equations for a double gap spoke PM vernier motor to obtain the back EMF, reactance and power factor considering a variety of factors. Subsequently the proper design procedure is applied for a case study. Finally, to validate the proposed equation and design method, various types of motors are simulated by using FEA and compared with the analytical results.

## II. THE STRUCTURE TO MAXIMIZE VERNIER EFFECT

### A. Review of Surface PM Structure [8 ]

A surface PM motor is shown in Fig. 1 which has the stator slot number $Z_s$, stator winding pole pairs $p$, the number of rotor magnet pairs $Z_r$ whose thickness is $g_m$, the angular position in air gap $\theta$ and rotor's angular position $\theta_m$. For general and vernier PM machines with full pitch winding, the stator slots $Z_s$ can be expressed by $6pq$ where $q$ is the number of slots per pole and phase. When a condition for relation between rotor-magnet pairs $Z_r$ and stator slots $Z_s$ is met, substantial back-EMF is developed in addition to the common EMF of PM machine, which is vernier effect. The MMF developed by surface PM $F_{PM}$ and the specific air gap permeance $P$ are expressed by (1) and (2) respectively where $B_r$ is the residual flux density of PM, the quantities $P_0$ and $P_1$ are the average and 1st harmonic specific permeance of air gap in Fourier series expression. The air gap flux density $B(\theta)$

This article has been accepted for publication in a future issue of this journal, but has not been fully edited. Content may change prior to final publication. Citation information: DOI 10.1109/TIA.2015.2477798, IEEE Transactions on Industry Applications

which is the product of (1) and (2) is given by (3).

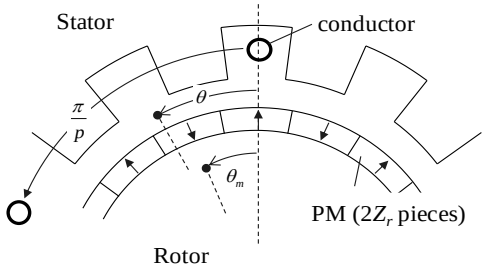


Fig. 1 Portion of PM vernier motor geometry

$$F_{PM}(\theta,\theta_m) \approx \frac{4}{\pi}\frac{g_m}{\mu_m} B_r \cos Z_r(\theta-\theta_m) \tag{1}$$

$$P(\theta) \approx P_0 - P_1 \cos(Z_s\theta) \tag{2}$$

$$B(\theta) = \frac{4}{\pi}\frac{g_m}{\mu_m} B_r \left\{ \begin{array}{l} P_0 \cos Z_r(\theta-\theta_m) \\ -\frac{P_1}{2}\left( \begin{array}{l} \cos\left((Z_r - Z_s)\theta - Z_r\theta_m\right) \\ +\cos\left((Z_r + Z_s)\theta - Z_r\theta_m\right) \end{array} \right) \end{array} \right\} \tag{3}$$

For a conventional PM machine, the back-EMF due to the flux densities with $Z_r \mp Z_s$ in (3) is negligible. However, the term $Z_r$ - $Z_s$ in (3) plays a key role in boosting back-EMF in a vernier motor. When a full pitch coil with single turn meets the necessary condition $Z_r$ - $Z_s$ = -$p$, alternatively $Z_r$ = $p$(6$q$-1), the induced voltage of the coil can be obtained by (4) where $D_g$ is the air gap diameter, $l_{stk}$ is the stack length of core, and $\omega_m$ is a mechanical rotor speed.

$$\begin{aligned} e_i(t) &= \frac{d\theta_m}{dt}\frac{d\phi_i(\theta_m)}{d\theta_m} \\ &= \frac{D_g l_{stk}\omega_m}{2}\int_{\theta_i}^{\theta_i+\frac{\pi}{p}} \frac{d}{d\theta_m} B(\theta,\theta_m)\, d\theta \\ &\approx D_g l_{stk}\omega_m \frac{4}{\pi}\frac{g_m}{\mu_m} B_r \left(P_0 + \frac{6q-1}{2}P_1\right)\cos\left(Z_r\omega_m t + p\theta_i\right) \end{aligned} \tag{4}$$

By using (4), the back-EMF(rms) of a phase winding with $q$ slots/pole/phase is obtained by (5) where $N_{ph}$ is the total series turns of the winding and $k_w$ is a winding factor.

$$\begin{aligned} E_{ph} &= \mathrm{RMS}\left(\frac{N_{ph}}{q}\sum_{i=1}^{q} e_i(t)\right) \\ &= \frac{k_w N_{ph} D_g l_{stk}\omega_m}{\sqrt{2}}\left\{\frac{4}{\pi}\frac{g_m}{\mu_m} B_r\left(P_0 + \frac{6q-1}{2}P_1\right)\right\} \end{aligned} \tag{5}$$

In the back EMF equation (5), the first term with $P_0$ is developed through the same principle as that of the conventional PM machine, but the second with $P_1$ is a unique voltage produced by harmonic modulation, that is, the vernier effect. Consequently, the voltage boost in the vernier motor is achieved by the $P_1$ even though it is less than $P_0$. The permeance $P_0$ and $P_1$ are expressed in terms of geometries of slot and air gap as follows

$$P_0 = \frac{\mu_0}{g}(1 - 1.6\beta c_0) \tag{6}$$

$$P_1 = \frac{\mu_0}{g}\frac{2\beta}{\pi}\left(\frac{0.78}{0.78 - 2c_0^{\,2}}\right)\sin(1.6\pi c_0), \tag{7}$$

where $g$ in (6) and (7) is the magnetic length of the gap between rotor and stator, that is, the sum of air gap length $g_a$ and the effective length of magnet thickness $g_m/\mu_m$ for a surface PM machine.

The coefficient $c_0$ in (6) is the ratio of stator slot opening $o$ to slot pitch $t_d$ and should be roughly 0.5~0.6 to obtain a maximum value of $P_1$ [8]. The coefficient $\beta$ is a nonlinear function of $o/g$, whose maximum value is less than 0.5 as shown in Fig. 2. In order to obtain a high back EMF, it is necessary to pay attention to $\beta$ because the value of $P_0$+(6$q$-1)$P_1$/2 in (5) is proportional to $\beta$ when $c_0$ and $q$ are determined and fixed. In other words, from the Fig. 2, it can be seen that as $o/g$ becomes higher, the back EMF becomes higher. As mentioned above, however, $g$ is the sum of $g_a$ and $g_m/\mu_m$ for a surface PM motor, so that the magnet thickness $g_m$ should be very thin to obtain a high value of $o/g$, which may cause a high risk of demagnetization of magnet as well as poor power factor due to high reactance.

Therefore, the above equations suggest the following. If the magnet is buried into rotor core, $o/g$ and back EMF would increase regardless of the thickness of magnet, and the demagnetization problem would be also avoided. Hence, a spoke PM rotor was selected as a suitable structure.

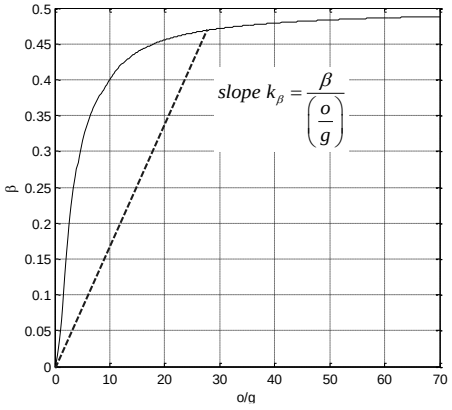


Fig. 2 Parameter $\beta$ versus $o/g$

### *B. Problem of Spoke PM Machine with a Single Air Gap*

A spoke PM vernier motor with a single-gap outer stator is shown in Fig. 3, which has a general spoke PM structure except for a specific combination of $Z_s$ and $Z_r$ to get vernier effects. Considering the spoke structure with a small gap between stator and rotor (the gap length exaggerated in the

This article has been accepted for publication in a future issue of this journal, but has not been fully edited. Content may change prior to final publication. Citation information: DOI 10.1109/TIA.2015.2477798, IEEE Transactions on Industry Applications

Fig. 3), it is readily expected that $P_0$ and $P_1$ in (6) and (7) will be larger than those of a surface PM motor. In order to calculate the air gap flux density, the magnetic potential of rotor core should be known. It should be noted that unlike the surface PM machine, the rotor core in Fig. 3 is divided into many pieces. Therefore the potential of each piece is magnetically floating and the magnetic potential of each piece should be first calculated. To this end, the magnetic equivalent circuit in Fig 4 can be constructed, where $F_{mag}$ is the MMF of magnet $(B_r/\mu_m)g_m$, $V_k$ is the potential of $k^{th}$ core piece. $R_m$ and $\bar{P}_{g.k}$ are the lumped reluctance of a magnet and the lumped air gap permeance facing with the $k^{th}$ core piece, which are given by (8) and (9) respectively.

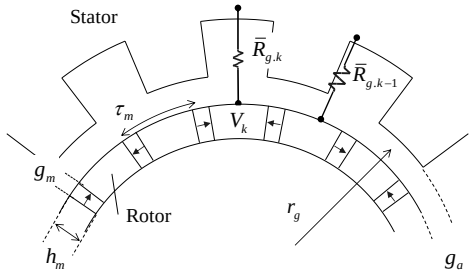

Fig. 3 Single gap spoke PM vernier motor

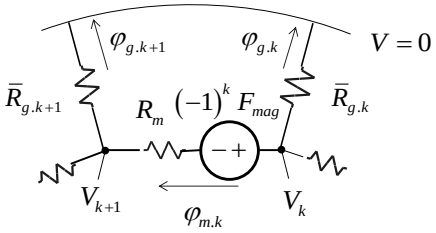

Fig. 4 Magnetic equivalent circuit

$$R_m = \frac{g_m}{\mu_m h_m l_{stk}} = \frac{g_m}{\mu_m A_m} \tag{8}$$

$$\begin{aligned}\bar{P}_{g.k} &= r_g l_{stk}\int_{\theta_{r.k}-\Delta}^{\theta_{r.k}+\Delta} P(\theta)\,d\theta_r \\ &= r_g l_{stk}\int_{\theta_{r.k}-\Delta}^{\theta_{r.k}+\Delta} P_o - P_1\cos Z_s(\theta_r+\theta_m)\,d\theta_r \\ &= \bar{P}_0 - \bar{P}_1\cos Z_s(\theta_{r.k}+\theta_m)\end{aligned} \tag{9}$$

,where

$$\Delta = \frac{\pi}{2Z_r},\ \bar{P}_0 = A_g P_o,\ \bar{P}_1 = \frac{\sin(\Delta Z_s)}{\Delta Z_s} A_g P_1 \text{ and } A_g = 2r_g l_{stk}\Delta.$$

As the permeance $\bar{P}_{g.k}$ in (9) varies with rotor position, so does the potential $V_k$. Thus, it is reasonable for the potential $V_k$ to have a form similar to the permeance (9). The expression is given by (10) where $\chi_1$ is as yet unknown.

$$\begin{aligned}V_k(\theta_{r.k}) &= (-1)^k\left(\frac{F_{mag}}{4+R_m\bar{P}_0} - \chi_1\cos Z_s(\theta_{r.k}+\theta_m)\right) \\ &= (-1)^k\,\Phi_k\end{aligned} \tag{11}$$

By using (10) as well as the relations from Fig. 4 $\varphi_{g.k} = \varphi_{m.k-1} - \varphi_{m.k}, V_k = \varphi_{g.k}/\bar{P}_{g.k}$, the potential equation (11) is obtained. One can then obtain the magnetic potential $V_k$ of (12) by solving (11), where the binomial theorem is used.

$$2F_{mag} = \Phi_{k-1} + \left(2+R_m\bar{P}_{g.k}\right)\Phi_k + \Phi_{k+1} \tag{11}$$

$$\begin{aligned}V_k &\approx (-1)^k\frac{2F_{mag}}{4+R_m\bar{P}_{g.k}} \\ &\approx (-1)^k\frac{2F_{mag}}{4+R_m\bar{P}_0}\left(1+\frac{R_m\bar{P}_1}{4+R_m\bar{P}_0}\cos Z_s(\theta_{r.k}+\theta_m)\right)\end{aligned} \tag{12}$$

The cosine term of (12) shows that the potential of rotor core piece oscillates as the rotor rotates. The air gap MMF distribution (13) is easily obtained by replacing $(-1)^k$ in (12) with $(4/\pi)\cos Z_r\theta_r$. It can be seen that the MMF is basically a rotating field, but the magnitude of field is pulsating as the rotor rotates. The result is a very unique feature of single gap vernier spoke PM machine, which ultimately produces critical problems in the flux density and back EMF characteristics, as demonstrated below.

$$F_{PM}(\theta) = \frac{8}{\pi}\frac{F_{mag}}{4+R_m\bar{P}_0}\left(1+\frac{R_m\bar{P}_1}{4+R_m\bar{P}_0}\cos Z_s\theta\right)\cos Z_r(\theta-\theta_m) \tag{13}$$

To obtain the air gap flux density, $P_{eff}(\theta)$ the product of the parenthesis in MMF (13) and the specific permeance $P(\theta)$, is first calculated by using the relation $\bar{P}_1/\bar{P}_0 = P_1/P_0$ and neglecting high harmonics and shown as the following.

$$\begin{aligned}P_{eff}(\theta) &= \left(1+\frac{R_m\bar{P}_1}{4+R_m\bar{P}_0}\cos Z_s\theta\right)(P_0 - P_1\cos Z_s\theta) \\ &\approx P_0\left(1-\frac{1}{2}\left(\frac{\bar{P}_1}{\bar{P}_0}\right)^2\frac{R_m\bar{P}_0}{4+R_m\bar{P}_0}\right) \\ &\quad -P_1\left(1-\frac{R_m\bar{P}_0}{4+R_m\bar{P}_0}\right)\cos Z_s\theta\end{aligned} \tag{14}$$

For the spoke structure, both values of the $R_m$ and $\bar{P}_0$ in (14) are quite large, so that $R_m\bar{P}_0/(4+R_m\bar{P}_0)$ is close to unity. On the other hand, $(\bar{P}_1/\bar{P}_0)^2$ has a quite small value, which makes $P_{eff}(\theta) \approx P_0$. Since $F_{mag}$ is the MMF of magnet $(B_r/\mu_m)g_m$, the flux air gap density is finally given by (15).

$$B(\theta) \approx \frac{4}{\pi}\frac{B_r}{\mu_m}\frac{2g_m P_0}{4+R_m\bar{P}_0}\cos Z_r(\theta-\theta_m) \tag{15}$$

From (15), it can be seen that comparing (3) the magnitude of flux density increases with the spoke structure. However,

This article has been accepted for publication in a future issue of this journal, but has not been fully edited. Content may change prior to final publication. Citation information: DOI 10.1109/TIA.2015.2477798, IEEE Transactions on Industry Applications

the flux component related with $P_1$ producing the vernier effect does not exist, which is caused by this feature. Even though the permeance $P_1$ in the spoke structure is much higher than that in a surface PM, the advantage is cancelled out by the potential oscillation in the rotor core, making it more difficult to obtain a high back EMF.

### *C. Double Gap Spoke PM Vernier Machine*

The crucial problem of the single air gap spoke type machine is the potential oscillation of core pieces which is basically produced by the oscillation of the air gap permeance facing with the core piece when rotor rotates. Thus, to avoid this effect, a proposed double gap structure as shown in Fig. 5 is suggested. In this figure, the inner stator is shifted by one slot pitch compared to the outer stator, where the outer and inner gap specific permeance, $P_g^+(\theta)$ and $P_g^-(\theta)$ are given in (16).

$$P_g^{\pm}(\theta) = P_0^{\pm} \mp P_1^{\pm} \cos Z_s\theta \tag{16}$$

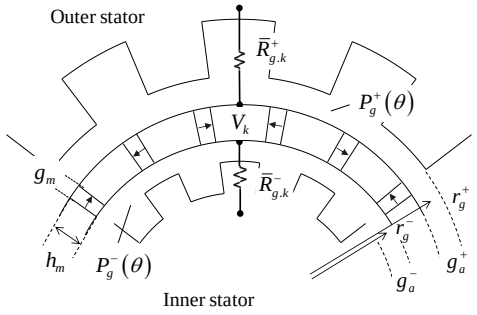


Fig. 5 Double gap spoke PM vernier motor

The lumped permeance values of both gaps are obtained by (17). Because both permeance are parallel to the core rotor core piece, the magnetic circuit for the rotor can be constructed as in Fig. 6 and the resulting permeance of a core piece is given by (18).

$$\begin{aligned}\bar{P}_{g.k}^{\pm} &= l_{stk} r_g^{\pm} \int_{\theta_k-\Delta}^{\theta_k+\Delta} P_g^{\pm}(\theta)\, d\theta_r \\ &= \bar{P}_0^{\pm} \mp \bar{P}_1^{\pm} \cos Z_s(\theta_{r.k} + \theta_m)\end{aligned} \tag{17}$$

where $\bar{P}_0^{\pm} = A_g^{\pm} P_0^{\pm}$ , $\bar{P}_1^{\pm} = \dfrac{\sin(\Delta Z_s)}{\Delta Z_s} A_g^{\pm} P_1^{\pm}$ and $A_g^{\pm} = 2 l_{stk} r_g^{\pm} \Delta$ .

$$\begin{aligned}\bar{P}_{g.k\,\Pi} &= \bar{P}_{g.k}^{+} + \bar{P}_{g.k}^{-} \\ &= \bar{P}_0^{+} + \bar{P}_0^{-} - \left(\bar{P}_1^{+} - \bar{P}_1^{-}\right)\cos Z_s(\theta_{r.k} + \theta_m)\end{aligned} \tag{18}$$

To eliminate the potential oscillation in the core piece, the term $(P_1^+ - P_1^-)$ in (18) should disappear in which case one obtains (19) from (17). When $c_0$ (the ratio of slot open to slot pitch) in (6) and (7) is set to the same value for both stators, one again obtains condition (20) from (19).

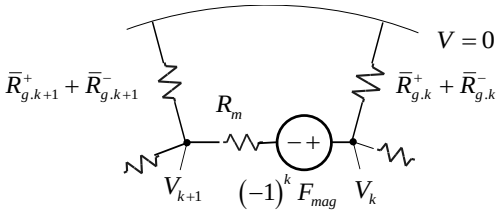


Fig. 6 Magnetic equivalent circuit

$$r_g^+ P_1^+ = r_g^- P_1^- \tag{19}$$

$$\frac{r_g^+}{g_a^+}\beta^+ = \frac{r_g^-}{g_a^-}\beta^- \tag{20}$$

In (20), $\beta$ is the value determined by $o/g$ ($=c_0 r_g/Z_r g$). That is when $r_g^+/g_a^+ = r_g^-/g_a^-$, one obtains $\beta^+ = \beta^-$ and one can meet (20). Finally the following can be concluded. To remove the potential oscillation in the double gap spoke PM vernier motor, the same slot open ratios $c_0$ and the same $r/g$ are needed for both gaps. Under these conditions, the net permeance of (18) becomes (21) by using (17), where $\bar{P}_0^+ = \bar{P}_0^- = \bar{P}_0$. By analyzing the circuit of Fig. 6, one obtains the potential $V_k$ as shown in (22).

$$\begin{aligned}\bar{P}_{g.k\,\Pi} &= l_{st}\frac{\pi}{Z_r}\left(r_g^+ P_0^+ + r_g^- P_0^-\right) = 2\mu_0 l_{stk}\frac{\pi}{Z_r}\gamma\left(1 - 1.6\beta c_0\right) \\ &= 2\bar{P}_0\end{aligned} \tag{21}$$

$$V_k = (-1)^k \frac{F_{mag}}{2 + R_m \bar{P}_0} \tag{22}$$

By replacing $(-1)^k$ in (22) with $(4/\pi)\cos Z_r\theta_r$, one obtains the rotating MMF and flux density in air gap given by (23) and (24) in which there is no term creating an oscillation in the MMF and no loss of permeance. Thus it is expected that the vernier effect is maximally utilized.

$$F_{g.PM}^{\pm}(\theta) = \frac{4}{\pi}\frac{F_{mag}}{2 + R_m\bar{P}_0}\cos\left(Z_r(\theta - \theta_m)\right) \tag{23}$$

$$B^{\pm}(\theta) = \frac{4}{\pi}\frac{B_r}{\mu_m}\frac{g_m}{2 + R_m\bar{P}_0}\cos Z_r(\theta - \theta_m)\left(P_0^{\pm} \mp P_1^{\pm}\cos Z_s\theta\right) \tag{24}$$

On the other hand, it should be noticed that if the same magnet are used for the both single and double gap machines, the magnitude of flux density in (24) is less than that of single gap machine in (15). It is natural, however, because for the double gap machine, more flux in total is produced from magnet, causing a larger potential drop in magnet, and is ultimately divided into both air gaps.

## III. CHARACTERISTIC EQUATIONS

For the conventional and vernier motor with surface PM as well as the double gap vernier motor with spoke PM, back EMF and power factor equations are derived for each motor

This article has been accepted for publication in a future issue of this journal, but has not been fully edited. Content may change prior to final publication. Citation information: DOI 10.1109/TIA.2015.2477798, IEEE Transactions on Industry Applications

to evaluate and compare their characteristics.

### A. Back-EMF Equations

With same the relation of (3) and (5), for the double gap vernier motor, the back EMF induced in the outer stator winding with $N_{ph}$ turns is obtained as (25) from (24).

$$E_{ph.spok} = \frac{l_{stk}\omega_m}{\sqrt{2}} D_g^+ k_w N_{ph} \left\{ \frac{4}{\pi} \frac{B_r}{\mu_m} \frac{g_m}{2 + R_m \bar{P}_0} \left( P_0^+ + \frac{6q-1}{2} P_1^+ \right) \right\} \quad (25)$$

The ratio $c_0$ in the specific permeance (6) and (7) to obtain the maximal back EMF is in the range 0.5~0.6. Then by using (6), (7) with $c_0$=0.5, (8) and (21), the back EMF (25) can be simplified as (26).

$$E_{ph.spok} = \frac{4 l_{stk}\omega_m}{\sqrt{2}\pi} B_r D_g^+ \left(k_w N_{ph}\right) \Lambda_{E.spok}, \quad (26)$$

where

$$\Lambda_{E.spok} = \left\{1 + \left(3q - 1.3\right)\beta\right\} \left( \mu_r \frac{2g_a^+}{g_m} + \frac{A_g^+}{A_m}\left(1 - 0.8\beta\right) \right)^{-1} \quad (27)$$

From (26), it can be seen that the magnitude of back EMF is proportional to the coefficient $\Lambda_{E.spok}$, that is, $q$, $g_m$, and $\beta$. Since $\beta$ in Fig. 2 is function of $o/g$ and $o$ is inversely proportional to $p$ and $q$, the back EMF will be larger with the less $p$, on the other hand, will be larger with larger $q$ due to the term (3$q$-1.3) in (27). With same procedure, the back EMF coefficient of a vernier and conventional motor with surface PM are obtained as (28) and (29) respectively from (6) and (7), where $c_0$ was set to 0.2 for the conventional surface PM and 0.5 for vernier surface PM.

$$\Lambda_{E.surf} = \left\{1 + \left(3q - 1.3\right)\beta\right\} \left( \mu_r \frac{g_a}{g_m} + 1 \right)^{-1} \quad (28)$$

$$\Lambda_{E.conv} = \left(1 - 0.3\beta\right) \left( \mu_r \frac{g_a}{g_m} + 1 \right)^{-1} \quad (29)$$

It is easily seen that the conventional motor's back EMF coefficient (29) is nearly independent with $p$ and $q$ and the least among (27)-(29) due to lack of vernier effect. In addition, since $\beta$ in (28) of surface PM is determined by the sum of magnet thickness $g_m$ and the air gap length, $\Lambda_{E.spok}$ of (27) is greater than $\Lambda_{E.surf}$ of (28) for the same $q$, which causes higher back EMF.

### B. Magnetizing Reactance Equations

The magnetic circuit seen from the outer stator winding of the double gap vernier motor has the structure of both air gaps connected in series. Therefore, the flux density in the both gaps produced by the MMF of 3-phase stator windings is given as (30) where $I_m$ is the peak stator current. Ignoring the leakage flux, the flux passing the gaps are same which means $r_g^+ B_g^+(\theta) = r_g^- B_g^-(\theta)$, then one can obtain the outer gap flux density (31) from (30). Consequently using (6) and the relation of $r_g^+ / g_a^+ = r_g^- / g_a^-$, the magnetizing inductance is obtained as (32).

$$\frac{3}{\pi} \frac{k_w N_{ph}}{p} I_m \sin p\theta = \frac{B_g^+(\theta)}{P_g^+(\theta)} + \frac{B_g^-(\theta)}{P_g^-(\theta)} \quad (30)$$

$$B_g^+(\theta) = \left( \frac{1}{P_g^+(\theta)} + \frac{r_g^+}{r_g^-} \frac{1}{P_g^-(\theta)} \right)^{-1} \frac{3}{\pi} \frac{k_w N_{ph}}{p} I_m \sin p\theta \quad (31)$$

$$\begin{aligned} L_{m.spok} &= \frac{k_w N_{ph}^+}{I_m} \int_0^{\frac{\pi}{p}} B_g^+(\theta) l_{stk} r_g^+ d\theta \\ &\approx \frac{6}{\pi} l_{stk} \frac{\left(k_w N_{ph}\right)^2}{p^2} \left( \frac{1}{r_g^+ P_0^+} + \frac{1}{r_g^- P_0^-} \right)^{-1} \\ &= \frac{6}{\pi} \mu_0 l_{stk} \frac{\left(k_w N_{ph}\right)^2}{p^2} r_g^+ \frac{1 - 0.8\beta}{2g_a^+} \end{aligned} \quad (32)$$

The magnetizing inductance of a vernier motor with single gap surface PM can be easily derived through the same procedure and given by (33) which can also be used for the inductance of conventional surface PM motor by replacing the coefficient 0.8 before $\beta$ with 0.3.

$$L_m = \frac{6}{\pi} \mu_0 l_{stk} \frac{\left(k_w N_{ph}\right)^2}{p^2} r_g \frac{1 - 0.8\beta}{g_a + \mu_r^{-1} g_m} \quad (33)$$

Both vernier and conventional motors with same winding pole-pairs $p$ have different the magnet pole pairs, so the operating frequencies are also different for a same rotational speed. The relation between electrical and mechanical frequency is $\omega_e = p\omega_m$ for conventional machine and $\omega_e = p(6q-1)\omega_m$ for vernier machine, thus using (32) and (33), the magnetizing reactance for each motor can be given by (34) and their coefficient (35)-(37) respectively. From (37), it should be noted that the reactance of a conventional machine depends on only $p$ and not on $q$, while those of vernier motors, (35) and (36) depend on both $p$ and $q$, which makes the reactance of vernier motor much higher. To be exact, the reactance gets larger with lager $q$ and smaller $p$, which is perfectly opposite to the back EMF characteristics of vernier motor. Thus it is necessary to find out the proper combination of $p$ and $q$ to meet high back EMF and power factor.

$$X_m = \frac{6}{\pi} \mu_0 \omega_m l_{stk} \left(k_w N_{ph}\right)^2 r_g \Lambda_X, \quad (34)$$

where the reactance coefficient of each model $\Lambda_X$ is as follows

This article has been accepted for publication in a future issue of this journal, but has not been fully edited. Content may change prior to final publication. Citation information: DOI 10.1109/TIA.2015.2477798, IEEE Transactions on Industry Applications

$$\Lambda_{X.spok} = \frac{1-0.8\beta}{2g_a^+} \cdot \frac{6q-1}{p} \tag{35}$$

$$\Lambda_{X.surf} = \frac{1-0.8\beta}{g_a + \mu_r^{-1} g_m} \cdot \frac{6q-1}{p} \tag{36}$$

$$\Lambda_{X.conv} = \frac{1-0.3\beta}{g + \mu_r^{-1} g_m} \cdot \frac{1}{p} \tag{37}$$

### C. Power Factor Equations

Since the resistance of machine is comparatively small, power factor is mainly determined by the back EMF and reactance voltage which consists of voltages of leakage and magnetizing reactance. Neglecting the leakage reactance and resistance, when the back EMF and the stator current are in phase, the power factor angle $\phi$ is given by (38) from (26) and (34).

$$\tan\phi = \frac{X_m I_{ph}}{E_{ph}} = \mu_0 \frac{3\left(k_w N_{ph}\right) I_{ph}}{2\sqrt{2} B_r} \frac{\Lambda_X}{\Lambda_E} \tag{38}$$

Generally the winding current $N_{ph}I_{ph}$ in (38) is limited by the max surface current density $K_s$ in (38), so the power factor can be represented by (40).

$$K_s = \frac{6 N_{ph} I_{ph}}{2\pi r_g} \tag{39}$$

$$\mathrm{PF} = \cos\left\{ \tan^{-1}\left( \frac{\pi}{2\sqrt{2}} \frac{\mu_0 k_w K_s r_g}{B_r} \frac{\Lambda_X}{\Lambda_E} \right) \right\} \tag{40}$$

## IV. Characteristic Analysis of The Double Air Gap Vernier Machine

### A. Characteristics Obtained by Analytical Equations

For the conventional and vernier motors with surface PM and the double gap vernier motor with spoke PM, the back EMF and power factor characteristics are analyzed and compared by using the derived equations. To these ends, the machines with $D_g$=400mm and $g_a$=3mm are investigated with various values $p$, $q$ and $g_m$. The surface current density is set to 14A/mm which is reasonable for small power machines. The magnet is assumed to be NdFeB with 1.1T of residual flux density $B_r$.

First, Fig. 7 shows the coefficient $\Lambda_{E.conv}$ and power factor for the conventional motor calculated with $q$=1, 2 and $p$=1~3, by (29), (37) and (40), where the magnet pole pairs $Z_r$ of conventional motor is same to the winding pole pairs $p$ regardless of $q$. It is seen that $\Lambda_{E.conv}$ increases and approaches to 1 as the magnet thickness $g_m$ increases, but it is nearly independent with $p$ and $q$ as shown in (29). However the power factor increases with $p$ and $g_m$ and easily goes above 0.9, and it is also independent with $q$, which is apparently explained with (37) and (40).

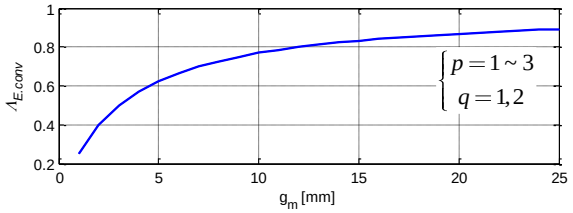


(a) Back EMF coefficient, $\Lambda_{E.conv}$ (when $q$=1 and 2)

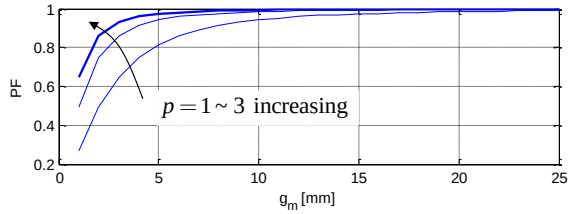


(b) Power factor (when $q$=1 and 2)

Fig. 7 Characteristics of a conventional SPM motor

Fig. 8(a)-(d) show the characteristics of a surface PM vernier motor with $q$=1, 2 and $p$=1~3 respectively. It should be noticed that unlike conventional machine, the magnet pole pairs $Z_r$ (= $p$(6$q$-1)) changes with $q$ as well as $p$. From Fig. 8(a) and (b) of $q$=1, more than 0.9 of power factor is achievable when $p$=2 or 3, but the back EMF coefficient $\Lambda_{E.surf}$ is less than 1.2, which means the advantage of vernier motor is weak. On the other hand, from Fig. 8(c) and (d) with $q$=2, $\Lambda_{E.surf}$ can be much higher than 1.5 when $p$=1, but the power factor is too low which is less than 0.75.

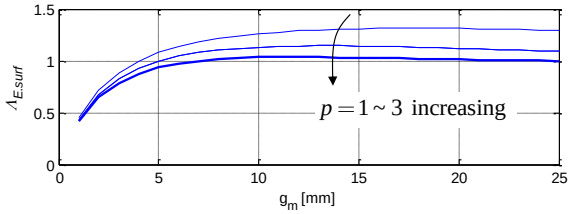


(a) Back EMF coefficient, $\Lambda_{E.surf}$ (when $q$=1)

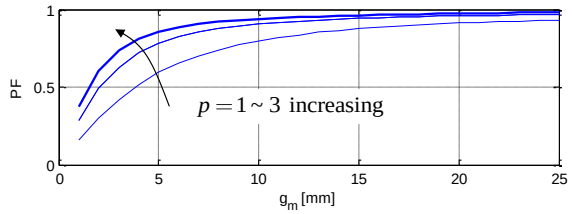


(b) Power factor (when $q$=1)

This article has been accepted for publication in a future issue of this journal, but has not been fully edited. Content may change prior to final publication. Citation information: DOI 10.1109/TIA.2015.2477798, IEEE Transactions on Industry Applications

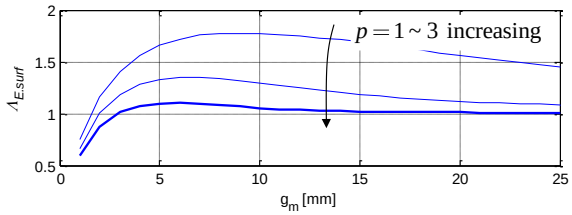


(c) Back EMF coefficient, $\Lambda_{E.surf}$ (when $q$=2)

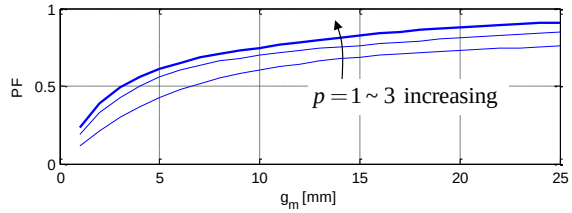


(d) Power factor (when $q$=2)

Fig. 8 Characteristics of a SPM vernier motor

Finally, Fig 9 represents the analysis results of a double gap spoke PM vernier motor. To analyze the characteristics, the ratio $A_m/A_g$ in (27) was set to 1 for fair comparison, and the maximum available magnet thickness was adjusted to 1/3 of a pole pitch of rotor which changes with $p$ and $q$. From Fig. 9(a) and (b) with $q$=1, it is seen that power factor 0.9 and more is achievable when $p$=1 and 2, and especially when $p$=2, the back EMF coefficient $\Lambda_{E.spok}$ is almost 2 with $g_m$=20mm. Fig. 9(c) and (d) with $q$=2 shows while the back EMF can be up to 3, the power factor is less than 0.75 in a whole area. Therefore the double gap spoke PM motor with $p$=2 and $q$=1 is the best choice considering the back EMF, that is, power density and power factor.

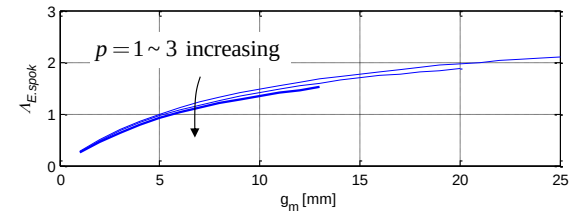


(a) Back EMF coefficient, $\Lambda_{E.spok}$ (when $q$=1)

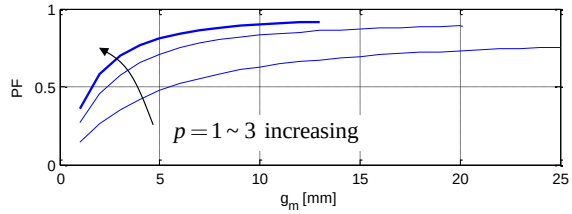


(b) Power factor (when $q$=1)

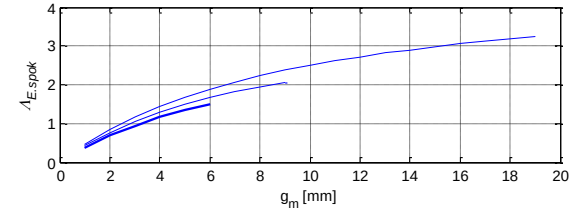


(c) Back EMF coefficient, $\Lambda_{E.spok}$ (when $q$=2)

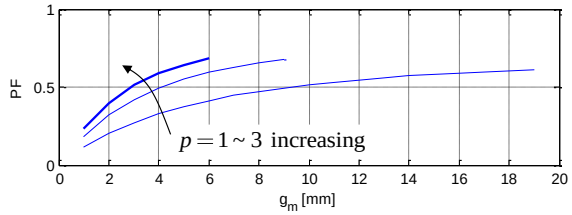


(d) Power factor (when $q$=2)

Fig.9 Characteristics of a double gap spoke PM vernier motor

### B. *Verification of Characteristics with FE-Analysis*

In order to validate the results from the analytic equations, FE analyses were performed for the conventional and vernier motor with surface PM, and the single and double gap vernier motor with spoke PM. To compare the simulation results clearly, specification of each model for simulation are different as given table I, where $\Lambda_E$ and PF for each model are included from the analytical results in Fig. 7-9. As shown in table I, the single gap vernier spoke PM motor is also included for analysis to verify the magnetic potential oscillation effects. The total number of turns is 32 and stack length is 50mm for every model.

TABLE I
SPECIFICATIONS FOR FE ANALYSIS MODELS &
ESTIMATED PERFORMANCE VALUES FROM DERIVED EQUATIONS

| | Conv. surface PM | Vern. surface PM | Vern. spoke PM 2-gap | Vern. spoke PM 1-gap |
|---|---|---|---|---|
| No. of $p$ | 2 | 1 | 2 | 2 |
| No. of $q$ | 2 | 2 | 1 | 1 |
| No. of $Z_r$ | 2 | 11 | 10 | 10 |
| $g_m$ [mm] | 20 | 10 | 20 | 20 |
| $\Lambda_E$ (estimated) | 0.87 | 1.77 | 1.9 | - |
| $\Lambda_X$ (estimated) | 25.5 | 659 | 257 | - |
| PF (estimated) | 0.99 | 0.60 | 0.89 | - |

The magnetic fields are simulated at 1000rpm with no load conditions, the flux distributions are represented in Fig. 10 and the back EMF characteristics are compared in Fig. 11. It can be seen that the surface PM vernier motor has more than 2 times of back EMF of conventional machine whose fundamental voltage is around 72V, as was predicted by comparing $\Lambda_{E.conv}$=0.87 and $\Lambda_{E.surf}$=1.77. It is also dramatic to compare the EMFs of spoke vernier machines. One can note that the single gap spoke PM vernier machine produces much less back EMF than the surface PM vernier machine, which is rather similar to that of conventional machine. On the other hand, the double gap machine reaches a slightly higher value than surface PM vernier motor does, as expected from $\Lambda_{E.spok}$ =1.9. To show cancelation of vernier effect in the single gap spoke motor, the air gap flux density waveforms and space harmonic composition of both spoke vernier motors with single and double gap are compared in Fig. 12. It should be noted the 5$^{th}$ harmonic is developed by MMF of PM itself but the 1$^{st}$ one is done by vernier effect ($Z_r$-$Z_s$=-$p$). The 1$^{st}$ component of single gap motor is much smaller than that of double gap motor, even though both motors have the same numbers of $p$ and $q$, which is due to the magnetic oscillation of rotor core piece.

This article has been accepted for publication in a future issue of this journal, but has not been fully edited. Content may change prior to final publication. Citation information: DOI 10.1109/TIA.2015.2477798, IEEE Transactions on Industry Applications

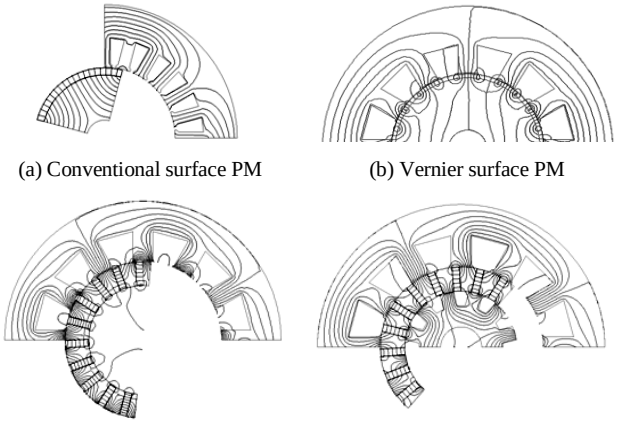

(a) Conventional surface PM (b) Vernier surface PM

(c) Vernier spoke PM with single gap (d) Vernier spoke PM with double gap

Fig.10 Flux distribution of FEA models with no loads

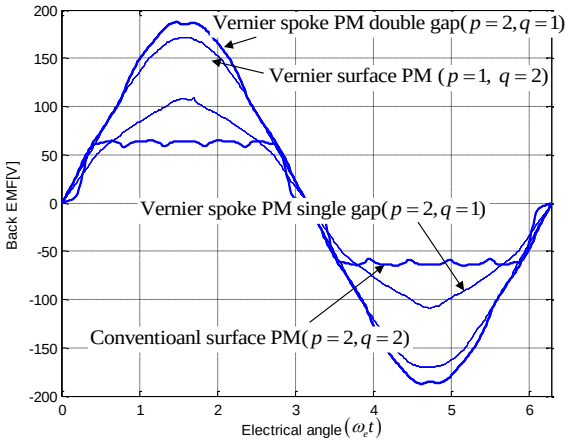


Fig.11 Back EMF characteristics with FEA(at 1000 rpm)

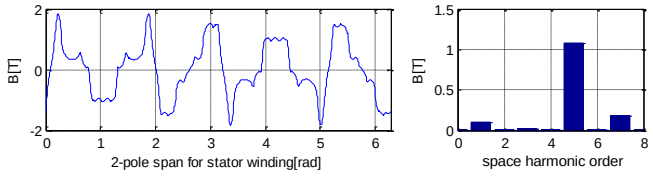


(a) Flux density of single gap motor

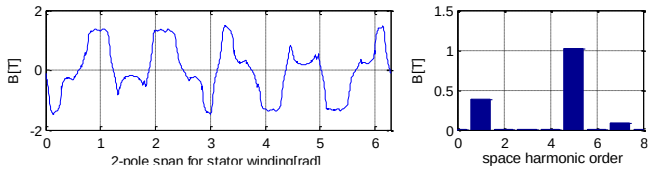


(b) Flux density of double gap motor

Fig.12 Air gap flux density waveforms and their harmonic magnitudes of spoke PM vernier motors

Next the phase voltage $V_{ind}$ induced in the winding and produced torque are simulated for each model at 1000rpm when a phase current is applied in phase with the back EMF. Neglecting the voltage drop due to small resistance and end-turn leakage, since $V_{ind}$ is same to the phase voltage, the power factor can be assumed as the difference between angles of $V_{ind}$ and applied current $I_{ph}$. The magnitude of a phase current is set 100A (rms) to meet the surface current density $K_s$=14A/mm. The induced voltage for a conventional PM motor is represented in Fig 13(a) which shows that the angle difference is almost zero, that is, the PF is nearly 1. Fig. 13(b) compares induced voltages and power factors of both vernier motors with surface and spoke PM. It is clearly seen that for the surface PM vernier motor, the magnitude of the induced voltage and the difference of angle between the voltage and the applied current of surface PM are much larger those of spoke PM vernier motor with double gaps. As the power factors for both motors are shown in Fig. 13(b), the values (0.91 and 0.63) are very close to the analytically estimated values (0.89 and 0.60) in table I, which proves the derived equations are very valid and the high power factor is obtainable in the vernier motor with a double gap spoke PM structure.

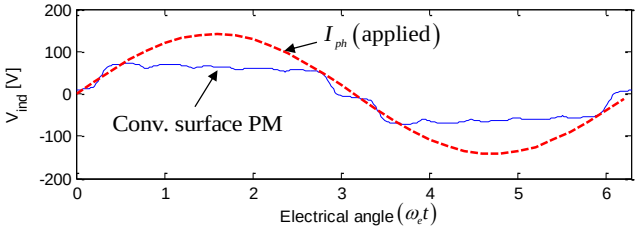


(a) Conventional surface PM motor

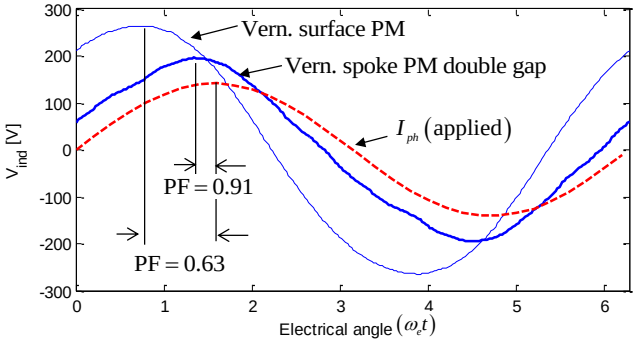


(b) Vernier surface PM and spoke PM motors

Fig.13 Power factor characteristics with FEA

Finally the torque characteristics are depicted in Fig. 14. As expected from the back EMF results, the torque values of the both vernier motors are more than twice of that of conventional PM motor, meaning the twice of power is obtained with a same motor volume. The large torque ripple of spoke PM motor with double gaps seems surprising because both inner and outer stator should cancel out the cogging torque produced in both gaps. It can be explained by the fact the magnet thickness for the inner stator surface should be thinner to cancel the ripples, but the magnet shape is actually parallel in the analytical model, making the flux densities of both gaps slightly unbalanced.

This article has been accepted for publication in a future issue of this journal, but has not been fully edited. Content may change prior to final publication. Citation information: DOI 10.1109/TIA.2015.2477798, IEEE Transactions on Industry Applications

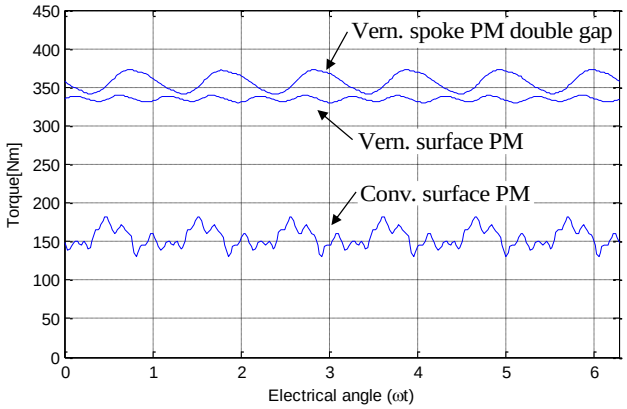

Fig.14 Torque characteristics with FEA

## V. CONCLUSION

In this paper, a spoke structure is applied to PM vernier motor in order to maximize the vernier effect increasing the back EMF. The inherent poor power factor of vernier motor due to high frequency operation is improved by controlling the winding pole number, which is very difficult for surface PM vernier motor. Initially the spoke PM with a single gap was investigated by using a magnetic equivalent circuit. However, phenomena was discovered which indicated that the increased vernier effects are substantially cancelled due to the magnetic potential oscillation in rotor core piece. To avoid such a magnetic oscillation, the spoke PM structure with double gap is proposed and various design conditions to maximize the vernier effects were provided. Using the magnetic investigation results, the reactance, power factor equations as well as back EMF equation are derived. To check the possibility of performance improvement in practical design, a machine with 400mm of gap diameter and 50mm stack length was assumed for a case study. With various variables such as winding poles $p$, stator slot numbers/phase/pole $q$ and the shape of the magnet, the maximum achievable power and power factor are calculated with the derived equations. From the calculated results, it was expected that the double gap spoke PM with $p$=2 and $q$=1 can provide more than the twice power of a conventional PM motor with the same volume and greater than 0.9 power factor. Finally, the estimated performance is verified with FE analysis.

## REFERENCES

[1] A. Toba and T.A. Lipo, "Novel Dual-Excitation Permanent Magnet Vernier Machine", Conference Record, 34th IAS Annual Meeting, 1999, pp. 2539-2544.

[2] J. Li, D. Wu, X. Zhang and S. Gao, "A New Permanent Magnet Vernier In-Wheel Motor for Electric Vehicles", Vehicle Power and Propulsion Conference (VPCC), 2010, pp. 1-6.

[3] S. L. Ho, S. Niu, and W. N. Fu, "Design and Comparison of Vernier Permanent Magnet Machines", IEEE Trans. On Magnetics, Vol. 47, No. 10, 2011, pp. 3280-3283.

[4] S. Niu, S. L. Ho, and W. N. Fu, "A Novel Direct-Drive Dual-Structure Permanent Magnet Machine", IEEE Trans. On Magnetics, Vol. 46, No. 6, 2010, pp. 2036-2039.

[5] H. Kakihata, Y. Katoka, and M. Takayma, "Design of Surface Permanent Magnet-type Vernier Motor", Electrical Machines and Systems, 2012, International Conference on.

[6] D. Li, R. Qu, "Sinusoidal Back-EMF of Vernier Permanent Magnet Machines", Electrical Machines and Systems, 2012, International Conference on, pp. 1-6

[7] K. Okada, N. Niguchi, and K. Hirata, "Aanlaysis of a Vernier Motor with Concentrated Windings", IEEE Trans. On Magnetics, Vol. 49. No. 5, 2013, pp.2241-2244

[8] B. Kim and T.A. Lipo, "Operation and Design Principles of a PM Vernier Motors", , IEEE Trans. On Industry Applications, Vol.50, No. 6, 2014, pp. 3656-3663.

[9] D. Li, R. Qu and T.A. Lipo, "High Power Factor Vernier Permanet Magnet Machines", in *Proc. IEEE Energy Conversion Congress & Exposition 2013*, (*ECCE*), pp. 1534-1540, Sept. 2013